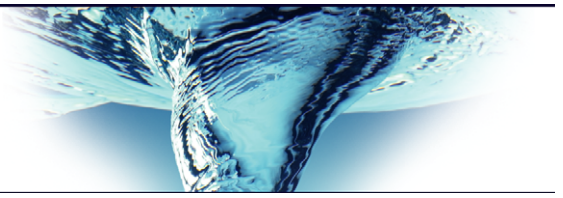
JFM RAPIDS
journals.cambridge.org/rapids



The electrophoretic mobility of rod-like particles

Ehud Yariv† and Ory Schnitzer

Department of Mathematics, Technion – Israel Institute of Technology, Haifa 32000, Israel

(Received 29 November 2012; revised 14 January 2013; accepted 16 January 2013)

At finite Dukhin numbers, where Smoluchowski's formula is inapplicable to thin-double-layer electrophoresis, the mobility of non-spherical particles is generally anisotropic. We consider bodies of revolution of otherwise arbitrary shape, where a uniformly applied electric field results in a rectilinear motion in the plane spanned by the field direction and the particle symmetry axis, as well as (for particles lacking fore–aft symmetry) rigid-body rotation about an axis perpendicular to that plane. Focusing upon slender particles, where the ratio ϵ of cross-sectional and longitudinal scales is asymptotically small, the translational and rotational mobilities are obtained as quadratures which depend upon the lengthwise distribution of the scaled cross-sectional width and the force densities associated with rigid-body motion. These mobility expressions approach finite limits as $\epsilon \to 0$, yielding closed-form expressions for specific particle geometries.

Key words: colloids, complex fluids, slender-body theory

1. Introduction

In the 'standard' thin-double-layer limit, the electrophoretic velocity is given by Smoluchowski's formula for all particle shapes (Morrison 1970). Numerical solutions of weak-field electrophoresis for arbitrary Debye widths (O'Brien & White 1978) depart however from that formula at moderately-large zeta potentials, even for very thin layers. This breakdown was explained by Derjaguin & Dukhin (1974) using a 'surface conduction' mechanism: in view of the Boltzmann-distributed ions within the thin diffuse layer, moderately-large zeta potentials results in high counter-ion concentration near the particle boundary. Under applied fields, effective 'surface' currents within the diffuse layer – normally negligible in the thin-double-layer limit – become significant, affecting in turn the electric-potential and salt-concentration distributions in the electro-neutral bulk. A linear macroscale model accounting for

† Email address for correspondence: udi@technion.ac.il

 © Cambridge University Press 2013
doi:10.1017/jfm.2013.43

https://doi.org/10.1017/jfm.2013.43 Published online by Cambridge University Press

surface conduction was presented by O'Brien (1983) and used to derive the mobility of a spherical particle. The mobility of a cylinder of identical radius turns out to be the same (Keh & Chen 1993).

As the irrotational-flow solution of Morrison (1970) no longer applies in the presence of surface conduction, the electrophoretic mobility of non-spherical particles is generally anisotropic, whereby particle velocity is not necessarily aligned with the field. Because of the technical difficulties involved, the only non-spherical particle shape addressed in that context is that of a spheroid (O'Brien & Ward 1988; Keh & Huang 1993). Even for such a simple shape no closed-form expressions are obtained for the mobility components, which are instead presented in tables and graphs. In this paper we derive mobility expressions for axisymmetric particles of otherwise arbitrary shape in the slender limit, which results in useful closed-form approximations.

The pioneering investigation of linear electrophoresis of slender bodies was carried out by Sherwood (1982) for arbitrary Debye thickness using a Henry-type analysis (see also Sherwood 1981). This was followed by the asymptotic analysis of Chen & Koch (1996*a*) of charged-fibre electrophoresis in the limit of thick Debye cloud (compared with fibre radius) – see also Chen & Koch (1996*b*) and Bach, Hollingsworth & Koch (2002). The thin-double-layer limit was analysed by Solomentsev & Anderson (1994) without surface conduction effects, where non-Smoluchowski velocities result from a non-uniform zeta-potential distribution. That limit was also addressed in the context of induced-charge electro-osmosis (Saintillan, Darve & Shaqfeh 2006; Yariv 2008), where the flow is quadratic in the applied field.

The present analysis is therefore complementary to that of Chen & Koch (1996*a*). As the slender limit is naturally encountered in modelling the electrophoresis of DNA (Allison, Chen & Stigter 2001), fibrous viruses (Kang & Dhont 2010; Buitenhuis 2012) and synthesized hematite particles (Rica, Jiménez & Delgado 2012), the importance of the present work goes beyond fundamental interest.

The linear weak-field model of O'Brien (1983) is expressed through the chemical potentials in the electro-neutral bulk. The present authors have recently derived a comparable macroscale model, not restricted to weak fields (Schnitzer & Yariv 2012), which is expressed through the electric potential and salt concentration. In what follows we will use the weak-field linearization of that model, where the relative role of surface conduction is expressed through a dimensionless Dukhin number. The related problem of diffusiophoresis, also addressed by Keh & Huang (1993) for spheroidal particles, can be analysed using a similar procedure.

2. Formulation

A dielectric particle of arbitrary shape and characteristic linear dimension a^* (dimensional quantities are hereafter decorated with an asterisk) is suspended in a binary electrolyte solution (permittivity ε^*, viscosity μ^*) of an unbounded extent. The electrolyte is symmetric, with ionic valencies $\pm\mathscr{Z}$ and identical equilibrium concentration c^* of cations and anions; the respective ionic diffusivities are denoted $D^{\pm *}$. The surface-charge density σ^* on the particle boundary is uniform; with no loss of generality we assume it positive. The particle–fluid system is exposed to a uniformly applied field of magnitude E^*. Our interest lies in the resulting rectilinear and angular electrophoretic motion. We focus upon the weak-field régime

$$\beta = \frac{a^* E^*}{\varphi^*} \ll 1; \tag{2.1}$$

https://doi.org/10.1017/jfm.2013.43 Published online by Cambridge University Press

here, $\varphi^* = k^*T^*/\mathscr{Z}e^*$ is the thermal voltage, wherein k^*T^* is the Boltzmann temperature and e^* the elementary charge.

With a view toward the eventual analysis of slender shapes, we allow for the existence of an additional length scale $b^* = \epsilon a^*$ (say with $\epsilon < 1$) characterizing the particle geometry. In addition to the geometric scales a^* and b^*, the governing equations also introduce a natural scale, the Debye width $1/\kappa^*$, κ^* being the Debye–Hückel parameter defined by $\kappa^{*2} = 2\mathscr{Z}e^*c^*/\varepsilon^*\varphi^*$. We address the electrokinetic transport in the limit where the diffuse portion of the double layer is much thinner than the smaller-scale b^* ($\kappa^*b^* \gg 1$). The governing differential equations then represent transport in the electro-neutral region surrounding the (polarized) Debye cloud, while the complementary conditions specified on the particle boundary $\mathscr{S}$ represent asymptotic matching with the quasi-equilibrium double-layer structure.

2.1. *Governing equations*

We employ the weak-field linearization of the generic macroscale model of Schnitzer & Yariv (2012). In what follows, length variables are normalized by a^*, the electric field by E^*, the electric potential by $\beta\varphi^*(=a^*E^*)$, and the salt concentration by βc^* (see (2.1)). In a laboratory frame, where the liquid at infinity is quiescent, the potential φ and the salt excess c are governed by Laplace's equation

$$\nabla^2\varphi = 0, \quad \nabla^2 c = 0; \tag{2.2a,b}$$

the boundary conditions on the (instantaneous) particle boundary

$$\frac{\partial c}{\partial n} + \frac{\partial \varphi}{\partial n} = 0, \quad \frac{\partial c}{\partial n} = \epsilon\, Du \nabla_s^2(\varphi - c), \tag{2.3a,b}$$

wherein $\partial/\partial n = \hat{\boldsymbol{n}}\cdot\boldsymbol{\nabla}$ is the normal derivative ($\hat{\boldsymbol{n}}$ being a normal unit vector pointing into the fluid) and ∇_s^2 the surface Laplacian; and the far-field conditions

$$\boldsymbol{\nabla}\varphi \to -\hat{\boldsymbol{E}}, \quad c \to 0, \tag{2.4a,b}$$

in which $\hat{\boldsymbol{E}}$ is a unit vector in the applied-field direction. For a given particle position, the problem (2.2)–(2.4) is independent of the engendered flow. Because of the linearity of that problem, the gradients of both φ and c are linear in $\hat{\boldsymbol{E}}$.

The parameter

$$Du = \frac{(1 + 2\alpha^-)\sigma}{\kappa^* b^*} \tag{2.5}$$

appearing in (2.3) is the Dukhin number associated with surface conduction on the smaller length scale of the particle. Here, $\sigma = \sigma^*/\varepsilon^*\varphi^*\kappa^*$ is the dimensionless surface-charge density, related to the 'particle zeta potential' ζ^* via the relation $\sigma = 2\sinh(\zeta/2)$, $\zeta = \zeta^*/\varphi^*$ being the dimensionless zeta potential. The parameter $\alpha^- = \varepsilon^*\varphi^{*2}/\mu^* D^{-*}$ is the ion-drag coefficient of the counter ions; for typical ionic diffusivities

$$\alpha^- \sim O(1) \tag{2.6}$$

(usually $\lesssim 0.5$, see Yariv, Schnitzer & Frankel 2011).

If the particle rotates the transport problem is unsteady and it may appear as though (2.2)–(2.3) require modifications. Note however that the ratio of the (largest) diffusive time scale a^{*2}/D^* (with D^* a characteristic ion diffusion coefficient, say D^{-*}) to the

https://doi.org/10.1017/jfm.2013.43 Published online by Cambridge University Press

time scale $\mu^* a^*/\varepsilon^*\zeta^* E^*$ associated with particle rotation is $O(\alpha^- \beta)$. In view of (2.6), the time scale ratio is asymptotically small in the present weak-field framework (2.1), justifying neglect of the temporal derivative term in (2.2*b*). Since the time scale $b^*/\kappa^* D^*$ associated with double-layer charging is even smaller, rotation also does not affect the boundary conditions (2.3).

When considering the electrokinetic flow it is convenient to employ Smoluchowski's scale $\varepsilon^*\zeta^* E^*/\mu^*$ for velocity variables. Angular velocities are accordingly normalized by $\varepsilon^*\zeta^* E^*/\mu^* a^*$. The associated scales for stress, force and torque variables are respectively provided by $\varepsilon^*\zeta^* E^*/a^*$, $\varepsilon^*\zeta^* a^* E^*$ and $\varepsilon^*\zeta^* a^{*2} E^*$. The fluid velocity $\boldsymbol{v}$ and pressure p are governed by the continuity and Stokes equations

$$\boldsymbol{\nabla}\cdot\boldsymbol{v} = 0, \quad \boldsymbol{\nabla} p = \nabla^2 \boldsymbol{v}, \tag{2.7a,b}$$

the far-field decay, $\boldsymbol{v} \to \boldsymbol{0}$ as $|\boldsymbol{x}| \to \infty$, and the boundary condition

$$\boldsymbol{v} = \boldsymbol{\nabla}_s \varphi + \Delta(\zeta)\boldsymbol{\nabla}_s c + \boldsymbol{u} + \boldsymbol{\omega}\times(\boldsymbol{x} - \boldsymbol{x}_O), \tag{2.8}$$

representing electro- and diffuso-osmotic slip on top of rigid-body motion. Thus, $\boldsymbol{\nabla}_s = \boldsymbol{\nabla} - \hat{\boldsymbol{n}}\,\partial/\partial n$ is the surface gradient operator, $\Delta(\zeta) = -(4/\zeta)\ln\cosh(\zeta/4)$, $\boldsymbol{u}$ is the velocity of a material point O within the particle (say its centroid), of instantaneous position $\boldsymbol{x}_O$, and $\boldsymbol{\omega}$ is the particle angular velocity. In addition to (2.7)–(2.8), the hydrodynamic force and torque engendered by the combination of osmotic slip and rigid-body motion must vanish when considering a freely suspended particle; these conditions serve to determine the rigid-body velocities $\boldsymbol{u}$ and $\boldsymbol{\omega}$. Note that electrical torques due to Maxwell stresses (see Yariv 2008) do not affect the present linearized weak-field approximation. In contrast to the common viewpoint, then, these particles rotate essentially due to surface conduction (see however (3.4) *et seq.*).

At moderate zeta potentials ($\zeta \sim O(1)$), the Dukhin number (2.5) is asymptotically small in the underlying thin-double-layer limit $\kappa^* b^* \gg 1$ (recall (2.6)). Salt polarization is then negligible (see (2.3*b*)), whereby the results of Morrison (1970) hold: the electro-osmotic flow is irrotational, $\boldsymbol{v} = \boldsymbol{\nabla}\varphi$, the particle translates with Smoluchowski's velocity, $\boldsymbol{u} = \hat{\boldsymbol{E}}$, and does not rotate. Our interest lies here accordingly in 'logarithmically large' zeta potentials, of order $2\ln(\kappa^* b^*)$. Then, $Du \sim O(1)$ in the limit $\kappa^* b^* \to \infty$ (see (2.5)), hence surface conduction enters the picture.

2.2. *Decomposition*

The linearity of the flow problem (2.7)–(2.8) suggests its decomposition into two separate problems respectively corresponding to the osmotic-slip and rigid-body-motion contributions to (2.8). In the first 'slip-driven' problem, where the particle is taken as stationary ($\boldsymbol{u} = \boldsymbol{0}$, $\boldsymbol{\omega} = \boldsymbol{0}$), (2.8) reads

$$\boldsymbol{v} = \boldsymbol{\nabla}_s \varphi + \Delta(\zeta)\boldsymbol{\nabla}_s c. \tag{2.9}$$

The linear dependence of $\boldsymbol{\nabla}\varphi$ and $\boldsymbol{\nabla} c$ upon $\hat{\boldsymbol{E}}$ implies a similar dependence of the slip-driven force and torque contributions, which accordingly possess the representations

$$\boldsymbol{f} = \boldsymbol{F}\cdot\hat{\boldsymbol{E}}, \quad \boldsymbol{g} = \boldsymbol{G}\cdot\hat{\boldsymbol{E}}, \tag{2.10a,b}$$

in which $\boldsymbol{F}$ is a second-order tensor and $\boldsymbol{G}$ a second-order pseudotensor. These coefficients are independent of $\hat{\boldsymbol{E}}$; they are functions of the particle geometry and orientation as well as the governing parameters ζ and Du. The second flow problem, engendered by rigid-body motion with no slip, results in the respective force and

https://doi.org/10.1017/jfm.2013.43 Published online by Cambridge University Press

torque contributions

$$\boldsymbol{R}\cdot\boldsymbol{u}+\boldsymbol{C}^{\dagger}\cdot\boldsymbol{\omega},\quad \boldsymbol{C}\cdot\boldsymbol{u}+\boldsymbol{S}\cdot\boldsymbol{\omega}, \tag{2.11}$$

wherein $\boldsymbol{R}$ and $\boldsymbol{S}$ are the second-order resistance tensors, $\boldsymbol{C}$ is the second-order coupling pseudotensor (Happel & Brenner 1965), and † denotes transposition. These coefficients are independent of $\boldsymbol{u}$ and $\boldsymbol{\omega}$.

A freely suspended particle satisfies the force- and torque-free conditions,

$$\boldsymbol{F}\cdot\hat{\boldsymbol{E}}+\boldsymbol{R}\cdot\boldsymbol{u}+\boldsymbol{C}^{\dagger}\cdot\boldsymbol{\omega}=\boldsymbol{0},\quad \boldsymbol{G}\cdot\hat{\boldsymbol{E}}+\boldsymbol{C}\cdot\boldsymbol{u}+\boldsymbol{S}\cdot\boldsymbol{\omega}=\boldsymbol{0}, \tag{2.12a,b}$$

whose inversion yields the electrophoretic velocities. As these are clearly linear in the applied field, they possess the representations

$$\boldsymbol{u}=\boldsymbol{U}\cdot\hat{\boldsymbol{E}},\quad \boldsymbol{\omega}=\boldsymbol{\Omega}\cdot\hat{\boldsymbol{E}}, \tag{2.13a,b}$$

where the translational electrophoretic mobility $\boldsymbol{U}$ (a second-order tensor) is generally anisotropic. (The rotational mobility $\boldsymbol{\Omega}$, being a second-order pseudotensor, is anisotropic by definition.)

3. Bodies of revolution

We consider bodies of revolution of (dimensional) length $2a^*$ and maximum (dimensional) width $2b^*$. The parameter ϵ then represents the particle slenderness. The particle orientation in space is defined by a unit vector $\hat{\boldsymbol{e}}$ attached to the symmetry axis. Since this is the single vector characterizing the system geometry, the only available second-order true tensors are $\boldsymbol{I}$ and $\hat{\boldsymbol{e}}\hat{\boldsymbol{e}}$. Thus, the second-order tensor coefficients possess the representations

$$\boldsymbol{F}=F^{\parallel}\hat{\boldsymbol{e}}\hat{\boldsymbol{e}}+F^{\perp}(\boldsymbol{I}-\hat{\boldsymbol{e}}\hat{\boldsymbol{e}}),\quad \boldsymbol{R}=R^{\parallel}\hat{\boldsymbol{e}}\hat{\boldsymbol{e}}+R^{\perp}(\boldsymbol{I}-\hat{\boldsymbol{e}}\hat{\boldsymbol{e}}),\quad \boldsymbol{S}=S^{\parallel}\hat{\boldsymbol{e}}\hat{\boldsymbol{e}}+S^{\perp}(\boldsymbol{I}-\hat{\boldsymbol{e}}\hat{\boldsymbol{e}}), \tag{3.1a,b,c}$$

as does the translational electrophoretic mobility

$$\boldsymbol{U}=U^{\parallel}\hat{\boldsymbol{e}}\hat{\boldsymbol{e}}+U^{\perp}(\boldsymbol{I}-\hat{\boldsymbol{e}}\hat{\boldsymbol{e}}). \tag{3.2}$$

Also, since the only available second-order pseudotensor is $\boldsymbol{\epsilon}\cdot\hat{\boldsymbol{e}}$ ($\boldsymbol{\epsilon}$ being the isotropic third-order pseudotensor) the second-order pseudotensor coefficients must possess the antisymmetric form

$$\boldsymbol{G}=-G\boldsymbol{\epsilon}\cdot\hat{\boldsymbol{e}},\quad \boldsymbol{C}=-C\boldsymbol{\epsilon}\cdot\hat{\boldsymbol{e}}, \tag{3.3a,b}$$

as must the mobility

$$\boldsymbol{\Omega}=-\Omega\boldsymbol{\epsilon}\cdot\hat{\boldsymbol{e}}. \tag{3.4}$$

The scalar coefficients appearing in the representations (3.1)–(3.4) are independent of the orientation $\hat{\boldsymbol{e}}$. They can only depend upon ζ, Du, and the intrinsic particle geometry.

In the case of a fore–aft-symmetric particle the necessary invariance under the transformation $\hat{\boldsymbol{e}}\rightarrow-\hat{\boldsymbol{e}}$ implies that both the slip-driven torque coefficient $\boldsymbol{G}$ and the coupling coefficient $\boldsymbol{C}$ vanish, as does the rotational mobility $\boldsymbol{\Omega}$. The present weak-field approximation thus does not predict rotation of fore–aft-symmetric particles. Their leading-order orientation is therefore determined by the 'dielectrophoretic' torque due to Maxwell stresses, not accounted for in the present linearized analysis. This torque results in particle rotation over the time scale $\mu^*/\varepsilon^*E^{*2}$, of order 1 s for $E^*\sim 10$ V cm^{-1} in aqueous solution. In the slender limit considered next, where that

https://doi.org/10.1017/jfm.2013.43 Published online by Cambridge University Press

torque scales as ϵ^2 (see Yariv 2008) and the resistance to rotation scales as $1/\ln\epsilon$ (see (7.4)), that time scale is further amplified by an $O(1/\epsilon^2\ln\epsilon)$ factor. Note that the Maxwell-stress torque itself is strongly affected by surface conduction, which modifies the particle dipole (Basuray, Wei & Chang 2010).

Substitution of (3.2) and (3.4) into (2.13) yields simplified expressions, still linear in $\hat{\boldsymbol{E}}$, for the particle velocities. Substitution of these together with (3.1) and (3.3) into the force- and torque-free conditions (2.12) while making use of the arbitrariness of $\hat{\boldsymbol{E}}$ yields the equations

$$F^{\parallel}+R^{\parallel}U^{\parallel}=0,\quad F^{\perp}+R^{\perp}U^{\perp}+C\Omega=0,\quad G+CU^{\perp}+S^{\perp}\Omega=0, \tag{3.5a,b,c}$$

whose inversion yields the scalar mobility coefficients. Note that the lateral mobility $U^{\perp}$ and rotational mobility Ω are coupled, whereas the longitudinal mobility $U^{\parallel}$ can be solved independently.

It is convenient to define a particle-fixed Cartesian system (x, y, z) where the x-axis lies along the symmetry axis, the y-axis lies in the plane spanned by $\hat{\boldsymbol{E}}$ and $\hat{\boldsymbol{e}}$, and the origin coincides with the centroid $\boldsymbol{x}_O$.The corresponding unit vectors are

$$\hat{\boldsymbol{e}}_x=\hat{\boldsymbol{e}},\quad \hat{\boldsymbol{e}}_y=\frac{\hat{\boldsymbol{E}}-\hat{\boldsymbol{e}}\cos\gamma}{\sin\gamma},\quad \hat{\boldsymbol{e}}_z=\frac{\hat{\boldsymbol{e}}\times\hat{\boldsymbol{E}}}{\sin\gamma}, \tag{3.6a,b,c}$$

wherein γ is the angle between the symmetry axis and the applied-field direction. Using (3.1) and (3.3) it then follows that the slip-driven force and torque (2.10) possess the form

$$\boldsymbol{f}=\hat{\boldsymbol{e}}_xF^{\parallel}\cos\gamma+\hat{\boldsymbol{e}}_yF^{\perp}\sin\gamma,\quad \boldsymbol{g}=\hat{\boldsymbol{e}}_zG\sin\gamma. \tag{3.7a,b}$$

As evident from (3.2) and (3.4), a similar form is possessed by the resulting electrophoretic velocities (2.13),

$$\boldsymbol{u}=\hat{\boldsymbol{e}}_xU^{\parallel}\cos\gamma+\hat{\boldsymbol{e}}_yU^{\perp}\sin\gamma,\quad \boldsymbol{\omega}=\hat{\boldsymbol{e}}_z\Omega\sin\gamma. \tag{3.8a,b}$$

With our definition of $2a^*$ as the (dimensional) particle length, the particle extends between $x=-1$ and $x=1$. In terms of cylindrical coordinates (r,θ,x) (where θ is measured counterclockwise from the y-axis in the yz plane), its boundary is given by

$$r=\epsilon\lambda(x),\quad -1<x<1. \tag{3.9}$$

With our definition of $2b^*$ as the maximum (dimensional) width, the maximum value of $\lambda(x)$ over $(-1, 1)$ is unity.

4. Slender particles

We now consider the slender limit

$$\epsilon\ll 1 \tag{4.1}$$

with $Du\sim O(1)$ (whereby surface conduction is appreciable on transverse scale). This limit is naturally analysed using inner–outer asymptotic expansions (Cox 1970). The 'outer' region, with r fixed as $\epsilon\to 0$, describes transport on the longitudinal scale, where the particle appears as a zero-thickness line segment. The 'inner' region, where $r\sim O(\epsilon)$ as $\epsilon\to 0$, describes processes occurring on the cross-sectional scale, where the particle appears as a slowly-varying infinite cylinder. The latter limit is facilitated

https://doi.org/10.1017/jfm.2013.43 Published online by Cambridge University Press

by the introduction of the stretched radial coordinate $\rho = r/\epsilon$. Note that

$$\frac{\partial}{\partial n} = \frac{1 + O(\epsilon^2)}{\epsilon}\left(\frac{\partial}{\partial \rho} - \epsilon^2 \frac{\mathrm{d}\lambda}{\mathrm{d}x}\frac{\partial}{\partial x}\right), \quad \nabla_s^2 \approx \frac{1}{\epsilon^2 \lambda^2}\frac{\partial^2}{\partial \theta^2}. \tag{4.2a,b}$$

Hereafter, the approximation symbol '$\approx$' implies a relative asymptotic error which is algebraically small in ϵ.

5. Calculation of c and φ

The linearity of the transport problem (2.2)–(2.4) suggests a superposition approach, considering first the case $\gamma = 0$, where the particle is aligned with the applied field, and then the case $\gamma = \pi/2$, where it is perpendicular to it.

5.1. *Aligned case*

In the outer region we postulate the asymptotic expansions

$$\varphi = -x + \tau(\epsilon)\tilde{\varphi} + \cdots, \quad c = \tau(\epsilon)\tilde{c} + \cdots, \tag{5.1a,b}$$

where the Poincaré pre-factor $\tau(\epsilon)$ remains to be determined. The perturbation $\tilde{\varphi}$ is represented as a line distribution of sources

$$\tilde{\varphi} = \frac{1}{4\pi}\int_{-1}^{1} \frac{s(\xi)\,\mathrm{d}\xi}{\sqrt{r^2 + (x-\xi)^2}}, \tag{5.2}$$

which automatically satisfy Laplace's equations and attenuation at infinity. A similar representation holds for $\tilde{c}$. At small r, $\tilde{\varphi} \sim -s(x)\ln r/2\pi$ (see Cole 1968).

In the inner region, conditions (2.3) in conjunction with the approximation (4.2*a*) suggest the expansion

$$\varphi = -x + \epsilon^2 \varphi_2(\rho, x) + \cdots, \tag{5.3}$$

while $c = o(\epsilon^2)$. Then, φ_2 is governed by the leading $O(1)$ balance of Laplace's equation and leading $O(\epsilon)$ balance of (2.3*a*), $\partial\varphi_2/\partial\rho = -\mathrm{d}\lambda/\mathrm{d}x$ at $\rho = \lambda(x)$. It therefore possesses the solution $\varphi_2 = -\lambda(\mathrm{d}\lambda/\mathrm{d}x)\ln\rho +$ a function of x. Asymptotic matching then implies $\tau = \epsilon^2$ and $s(x) = 2\pi\lambda\,\mathrm{d}\lambda/\mathrm{d}x$; it also necessitates the introduction of an $O(\epsilon^2\ln\epsilon)$ term (of magnitude $-\lambda\,\mathrm{d}\lambda/\mathrm{d}x$) into (5.3). Evidently, $\tilde{c} \equiv 0$. The solution is then the same as that obtained by Cole (1968) in the context of potential flow.

We are only interested in the leading $O(1)$ electric field and salt gradient on the boundary, which here simply read

$$\boldsymbol{\nabla}\varphi \approx -\hat{\boldsymbol{e}}_x, \quad \boldsymbol{\nabla}c \approx \boldsymbol{0}. \tag{5.4a,b}$$

Thus, the non-zero Dukhin number does not affect electrokinetic transport in this case. This was to be expected, as surface conduction in the longitudinal scale is an $O(\epsilon)$ effect.

5.2. *Perpendicular case*

In the outer region we postulate the expansions

$$\varphi = -r\cos\theta + \tau(\epsilon)\tilde{\varphi}(\rho, x, \theta) + \cdots, \quad c = \tau(\epsilon)\tilde{c}(\rho, x, \theta) + \cdots, \tag{5.5a,b}$$

https://doi.org/10.1017/jfm.2013.43 Published online by Cambridge University Press

wherein $\tilde{\varphi}$ is represented as a dipole distribution of magnitude $m(x)$

$$\tilde{\varphi} = \frac{r\cos\theta}{4\pi}\int_{-1}^{1}\frac{m(\xi)\,\mathrm{d}\xi}{[r^2+(x-\xi)^2]^{3/2}}. \tag{5.6}$$

A similar representation applies for $\tilde{c}$, say with dipole magnitude $n(x)$. Here at small r one readily obtains $\tilde{\varphi}\sim m(x)\cos\theta/2\pi r$ and $\tilde{c}\sim n(x)\cos\theta/2\pi r$.

The inner expansions now read

$$\varphi = -\epsilon\,[\rho+\varphi_1(\rho,x)]\cos\theta+\cdots, \quad c=\epsilon c_1(\rho,x)\cos\theta+\cdots. \tag{5.7a,b}$$

Laplace's equation at leading $O(\epsilon^{-1})$ in conjunction with the matching requirement yields $\varphi_1 = A(x)/\rho$ and $c_1 = B(x)/\rho$ (whereby $\tau=\epsilon^2$, $m(x)=2\pi A(x)$, and $n(x)=2\pi B(x)$). The leading $O(1)$ balances of conditions (2.3),

$$\frac{\partial\varphi_1}{\partial\rho}+\frac{\partial c_1}{\partial\rho}=1, \quad \frac{\partial c_1}{\partial\rho}=\frac{Du}{\lambda^2}(c_2+\rho-\varphi_1), \tag{5.8a,b}$$

obtained using (4.2*b*), yield $A=-\lambda^3/(\lambda+2Du)$ and $B=-2Du\lambda^2/(\lambda+2Du)$. We accordingly find the following $O(1)$ gradients at the particle boundary $\rho=\lambda$ (not bothering to calculate radial terms):

$$\boldsymbol{\nabla}\varphi\approx 2\hat{\boldsymbol{e}}_\theta\frac{\lambda(x)+Du}{\lambda(x)+2Du}\sin\theta+\hat{\boldsymbol{e}}_r(\cdots), \quad \boldsymbol{\nabla}c\approx 2\hat{\boldsymbol{e}}_\theta\frac{Du}{\lambda(x)+2Du}\sin\theta+\hat{\boldsymbol{e}}_r(\cdots). \tag{5.9a,b}$$

6. Slip-driven flow

For arbitrary inclination angle γ, the gradients of φ and c are obtained as a linear combination of (5.4) and (5.9). Since $\hat{\boldsymbol{n}}\,\partial/\partial n\approx\hat{\boldsymbol{e}}_r\,\partial/\partial r$ it is evident that the respective surface gradients are obtained, at the same level of approximation, by simply omitting radial terms. This yields

$$\boldsymbol{\nabla}_s\varphi\approx-\hat{\boldsymbol{e}}_x\cos\gamma+2\hat{\boldsymbol{e}}_\theta\frac{\lambda(x)+Du}{\lambda(x)+2Du}\sin\gamma\sin\theta, \tag{6.1a}$$

$$\boldsymbol{\nabla}_s c\approx 2\hat{\boldsymbol{e}}_\theta\frac{Du}{\lambda(x)+2Du}\sin\gamma\sin\theta. \tag{6.1b}$$

Using these expressions, we now consider the slip-driven flow animated by (2.9). In principle, it is possible to evaluate the velocity field $\boldsymbol{v}$ and the corresponding stress field $\boldsymbol{\Pi}$, integration of the latter providing the hydrodynamic loads acting on a stationary particle. Here, as in Yariv (2008), we avoid this procedure, employing instead a method due to Brenner (1964) which utilizes the Lorentz reciprocal relation (Happel & Brenner 1965),

$$\oint_{\mathscr{S}}\mathrm{d}A\,\hat{\boldsymbol{n}}\cdot\boldsymbol{\Pi}\cdot\bar{\boldsymbol{v}}=\oint_{\mathscr{S}}\mathrm{d}A\,\hat{\boldsymbol{n}}\cdot\bar{\boldsymbol{\Pi}}\cdot\boldsymbol{v}, \tag{6.2}$$

in which $\bar{\boldsymbol{v}}$ is any flow field that satisfies the Stokes equations and $\bar{\boldsymbol{\Pi}}$ the corresponding stress field. The requisite loads are obtained by choosing $\bar{\boldsymbol{v}}$ as the velocity field which corresponds to fictitious particle translation or rotation with a unit velocity. This method, which eliminates the need to calculate the slip-driven flow, is

https://doi.org/10.1017/jfm.2013.43 Published online by Cambridge University Press

natural for use here because solutions of the Stokes equations which correspond to rigid-body motion are already available for slender bodies (Cox 1970).

In view of (3.7) the slip-driven forces act in the x- and y-directions. To calculate the former we choose $\bar{\boldsymbol{v}}$ as the velocity field due to translation with a unit velocity in the x-direction. Substituting (2.9) and $\bar{\boldsymbol{v}}|_{\mathscr{S}} = \hat{\boldsymbol{e}}_x$ into (6.2) yields

$$\hat{\boldsymbol{e}}_x \cdot \oint_{\mathscr{S}} \mathrm{d}A\, \hat{\boldsymbol{n}} \cdot \boldsymbol{\Pi} = \oint_{\mathscr{S}} \mathrm{d}A\, \hat{\boldsymbol{n}} \cdot \bar{\boldsymbol{\Pi}} \cdot \{\nabla_s \varphi + \Delta(\zeta) \nabla_s c\}\,. \tag{6.3}$$

The left-hand side is the requisite force. The traction $\hat{\boldsymbol{n}} \cdot \bar{\boldsymbol{\Pi}}$ appearing in the right-hand side is provided by the solution of Cox (1970) for longitudinal particle translation,

$$\hat{\boldsymbol{n}} \cdot \bar{\boldsymbol{\Pi}} \approx \frac{\mathscr{F}^{\parallel}(x)}{2\pi\epsilon\lambda(x)} \hat{\boldsymbol{e}}_x, \tag{6.4}$$

wherein $\mathscr{F}^{\parallel}$ is the associated force per unit length in the x-direction exerted upon a particle translating with a unit velocity in that direction.

Similarly, the force in the y-direction is obtained by choosing $\bar{\boldsymbol{v}}$ as the velocity associated with a unit-velocity translation in that direction. Equation (6.3) applies again with $\hat{\boldsymbol{e}}_x$ replaced by $\hat{\boldsymbol{e}}_y$ in the left-hand side, which now represents the slip-driven hydrodynamic force in the y-direction. The traction $\hat{\boldsymbol{n}} \cdot \bar{\boldsymbol{\Pi}}$ appearing in the right-hand side, now associated with the flow due to lateral translation, is also provided by Cox (1970)

$$\hat{\boldsymbol{n}} \cdot \bar{\boldsymbol{\Pi}} \approx \frac{\mathscr{F}^{\perp}(x)}{2\pi\epsilon\lambda(x)} (\hat{\boldsymbol{e}}_\rho \cos\theta - \hat{\boldsymbol{e}}_\theta \sin\theta). \tag{6.5}$$

Here, $\mathscr{F}^{\perp}$ is the force per unit length in the y-direction which is exerted upon a particle translating with a unit velocity in that direction.

To obtain the torque about the z-axis we choose $\bar{\boldsymbol{v}}$ as the velocity field due to a fictitious rotation about that axis with a unit angular velocity. Substituting $\bar{\boldsymbol{v}}|_{\mathscr{S}} = \hat{\boldsymbol{e}}_z \times (\boldsymbol{x} - \boldsymbol{x}_O)$ and (2.9) into (6.2) yields

$$\hat{\boldsymbol{e}}_z \cdot \oint_{\mathscr{S}} \mathrm{d}A\, (\boldsymbol{x} - \boldsymbol{x}_O) \times (\hat{\boldsymbol{n}} \cdot \boldsymbol{\Pi}) = \oint_{\mathscr{S}} \mathrm{d}A\, \hat{\boldsymbol{n}} \cdot \bar{\boldsymbol{\Pi}} \cdot \{\nabla_s \varphi + \Delta(\zeta) \nabla_s c\}. \tag{6.6}$$

The left-hand side is the requisite torque. The field $\bar{\boldsymbol{v}}$ which corresponds to rigid-body rotation was calculated by Yariv (2008) using the method of Cox (1970). The traction associated with the unit-velocity rotation is of the form (6.5), but with $\mathscr{F}^{\perp}$ replaced by $\mathscr{F}^{\circlearrowleft}$, the force per unit length in the y-direction which is exerted upon a particle rotating with a unit velocity in the z-direction.

Substitution of (6.1) and performing the integrations readily provides the slip-driven loads. Comparison with (3.7) yields the coefficients

$$F^{\parallel} \approx -\int_{-1}^{1} \mathscr{F}^{\parallel}(x)\, \mathrm{d}x, \quad F^{\perp} \approx -\int_{-1}^{1} \mathscr{F}^{\perp}(x) \frac{\lambda(x) + Du + \Delta(\zeta) Du}{\lambda(x) + 2Du}\, \mathrm{d}x, \tag{6.7a,b}$$

$$G \approx -\int_{-1}^{1} \mathscr{F}^{\circlearrowleft}(x) \frac{\lambda(x) + Du + \Delta(\zeta) Du}{\lambda(x) + 2Du}\, \mathrm{d}x. \tag{6.7c}$$

In view of (3.1) and the definition of $\mathscr{F}^{\parallel}$, the first integral is simply $R^{\parallel}$.

https://doi.org/10.1017/jfm.2013.43 Published online by Cambridge University Press

7. Freely suspended particle

With the slip-induced loads calculated, the mobilities of a freely suspended particle are obtained from (3.5). Since $F^{\parallel} \approx -R^{\parallel}$ we find from (3.5*a*)

$$U^{\parallel} \approx 1. \tag{7.1}$$

This was to be expected since surface conduction is negligible on the longitudinal scale where the field is approximately uniform. The lateral and rotational mobilities are coupled through (3.5*b*,*c*). For $Du = 0$, where $F^{\perp} \approx -R^{\perp}$ and $G \approx -C$ (see (6.7*b*,*c*)), these readily yield $U^{\perp} \approx 1$ and $\Omega \approx 0$. Together with (7.1) these reproduce Smoluchowski's result.

When considering fore–aft-symmetric particles, which are already known not to rotate, the lateral balance (3.5*b*) yields $U^{\perp} = -F^{\perp}/R^{\perp}$. Substituting (6.7) then yields

$$U^{\perp} \approx \frac{1}{R^{\perp}} \int_{-1}^{1} \mathscr{F}^{\perp}(x) \frac{\lambda(x) + Du + \Delta(\zeta) Du}{\lambda(x) + 2Du} \, \mathrm{d}x. \tag{7.2}$$

The simplest case is that of a uniform width, $\lambda(x) \equiv 1$ (a finite cylinder). The integral is then proportional to $\int_{-1}^{1} \mathscr{F}^{\perp}(x) \, \mathrm{d}x = R^{\perp}$, and we find

$$U^{\perp} \approx \frac{1 + Du + Du\Delta(\zeta)}{1 + 2Du}, \tag{7.3}$$

which actually represents the transverse mobility of an infinite cylinder. Indeed, it is readily verified that (7.3) agrees with the mobility expression obtained by Keh & Chen (1993) in the corresponding two-dimensional problem, when terms $O(1/\kappa^* b^*)$ are omitted.

Going back to the general case described by (3.5*b*,*c*), a leading-order approximation may be obtained using the first term in the $\ln^{-1}\epsilon$ expansions of $\mathscr{F}^{\perp}$ and $\mathscr{F}^{\circlearrowleft}$. From Cox (1970) and Yariv (2008) we respectively find

$$\mathscr{F}^{\perp} \sim \frac{4\pi}{\ln \epsilon}, \quad \mathscr{F}^{\circlearrowleft} \sim \frac{4\pi x}{\ln \epsilon} \quad \left(\text{corresponding to } R^{\perp} \sim \frac{8\pi}{\ln \epsilon}, \; S^{\perp} \sim \frac{8\pi}{3 \ln \epsilon} \right). \tag{7.4a,b}$$

Since $C \sim O(\ln^{-2}\epsilon)$ (see Cox 1970) no coupling appears at $O(\ln^{-1}\epsilon)$. We readily find

$$U^{\perp} \sim \frac{1}{2} \int_{-1}^{1} \frac{\lambda(x) + Du + \Delta(\zeta) Du}{\lambda(x) + 2Du} \, \mathrm{d}x, \tag{7.5a}$$

$$\Omega \sim \frac{3}{2} \int_{-1}^{1} \frac{\lambda(x) + Du + \Delta(\zeta) Du}{\lambda(x) + 2Du} \, x \, \mathrm{d}x. \tag{7.5b}$$

Note that a finite mobility is approached as $\epsilon \to 0$ (as expected from the need to recover Smoluchowski's formula at $Du = 0$). Expression (7.5) is consistent with the general properties already observed, namely the nil rotation of fore–aft-symmetric particles (where $\lambda(x)$ is an even function) and the degeneration to Smoluchowski's formula at $Du = 0$.

The transverse mobility (7.5*a*) can be compared with the three solid curves provided in figure 5(*b*) of Keh & Huang (1993) for a spheroidal particle shape. In terms of the present notation, these mobility curves depict the variation of $U^{\perp}$ with the spheroid aspect ratio $a^*/b^* (= 1/\epsilon)$ for $\mathscr{Z} = 1$, 2 and 3. These curves were calculated for $\zeta^* = 5k^*T^*/e^*$ and $\kappa^* b^* = 300$, and accordingly correspond to $\zeta = 5$, 10 and 15 (where $Du = 0.0645$, 0.569, and 6.43). It appears that all three curves have practically

https://doi.org/10.1017/jfm.2013.43 Published online by Cambridge University Press

approached the respective slender limits at the largest aspect-ratio value ($1/\epsilon = 10$) provided; these limits are visually interpreted from the figure as 0.87, 0.45 and 0.14. Evaluation of $U^{\perp}$ using (7.5*a*) with $\lambda(x) = 1 - x^2$ yields

$$U^{\perp} \sim 1 - Du\frac{1 - \Delta(\zeta)}{2\sqrt{1 + 2Du}} \ln \frac{\sqrt{1 + 2Du} + 1 + Du}{Du}, \tag{7.6}$$

where the respective mobility values are 0.84, 0.44 and 0.14. The agreement at such a mild ϵ value, using a single term in a $1/\ln\epsilon$ expansion, is quite remarkable.

Acknowledgement

This work was supported by the Israel Science Foundation under grant no. 184/12.

References

ALLISON, S., CHEN, C. & STIGTER, D. 2001 The length dependence of translational diffusion, free solution electrophoretic mobility, and electrophoretic tether force of rigid rod-like model duplex DNA. *Biophys. J.* **81** (5), 2558–2568.

BACH, G. A., HOLLINGSWORTH, A. D. & KOCH, D. L. 2002 Electrophoretic mobility of rigid rodlike particles in dilute aqueous and glycerol suspensions: comparison between theory and experiment. *J. Colloid Interface Sci.* **251** (1), 208–213.

BASURAY, S., WEI, H. H. & CHANG, H.-C. 2010 Dynamic double layer effects on ac-induced dipoles of dielectric nanocolloids. *Biomicrofluidics* **4** (2).

BRENNER, H. 1964 The Stokes resistance of an arbitrary particle – IV. Arbitrary fields of flow. *Chem. Engng Sci.* **19**, 703–727.

BUITENHUIS, J. 2012 Electrophoresis of fd-virus particles: experiments and an analysis of the effect of finite rod lengths. *Langmuir* **28** (37), 13354–13363.

CHEN, S. B. & KOCH, D. L. 1996*a* Electrophoresis and sedimentation of charged fibres. *J. Colloid Interface Sci.* **180** (2), 466–477.

CHEN, S. B. & KOCH, D. L. 1996*b* Rheology of dilute suspensions of charged fibres. *Phys. Fluids* **8**, 2792.

COLE, J. D. 1968 *Perturbation Methods in Applied Mathematics*. Blaisdell.

COX, R. G. 1970 The motion of long slender bodies in a viscous fluid. Part 1. General theory. *J. Fluid Mech.* **44**, 791–810.

DERJAGUIN, B. V. & DUKHIN, S. S. 1974 Nonequilibrium double layer and electrokinetic phenomena. In *Electrokinetic Phenomena* (ed. E. Matijevic). *Surface and Colloid Science*, vol. 7, pp. 273–336. John Wiley.

HAPPEL, J. & BRENNER, H. 1965 *Low Reynolds Number Hydrodynamics*. Prentice-Hall.

KANG, K. & DHONT, J. K. G. 2010 Electric-field induced transitions in suspensions of charged colloidal rods. *Soft Matt.* **6** (2), 273–286.

KEH, H. J. & CHEN, S. B. 1993 Diffusiophoresis and electrophoresis of colloidal cylinders. *Langmuir* **9** (4), 1142–1149.

KEH, H. J. & HUANG, T. Y. 1993 Diffusiophoresis and electrophoresis of colloidal spheroids. *J. Colloid Interface Sci.* **160** (2), 354–371.

MORRISON, F. A. 1970 Electrophoresis of a particle of arbitrary shape. *J. Colloid Interface Sci.* **34**, 210–214.

O'BRIEN, R. W. 1983 The solution of the electrokinetic equations for colloidal particles with thin double layers. *J. Colloid Interface Sci.* **92** (1), 204–216.

O'BRIEN, R. & WARD, D. 1988 The electrophoresis of a spheroid with a thin double layer. *J. Colloid Interface Sci.* **121** (2), 402–413.

O'BRIEN, R. W. & WHITE, L. R. 1978 Electrophoretic mobility of a spherical colloidal particle. *J. Chem. Soc., Faraday Trans.* **74**, 1607–1626.

https://doi.org/10.1017/jfm.2013.43 Published online by Cambridge University Press

RICA, R. A., JIMÉNEZ, M. L. & DELGADO, Á. V. 2012 Electrokinetics of concentrated suspensions of spheroidal hematite nanoparticles. *Soft Matt.* **8** (13), 3596–3607.

SAINTILLAN, D., DARVE, E. & SHAQFEH, E. S. G. 2006 Hydrodynamic interactions in the induced-charge electrophoresis of colloidal rod dispersions. *J. Fluid Mech.* **563**, 223–259.

SCHNITZER, O. & YARIV, E. 2012 Macroscale description of electrokinetic flows at large zeta potentials: nonlinear surface conduction. *Phys. Rev.* E **86**, 021503.

SHERWOOD, J. D. 1981 Primary electroviscous effect in a suspension of rods. *J. Fluid Mech.* **111**, 347–366.

SHERWOOD, J. D. 1982 Electrophoresis of rods. *J. Chem. Soc., Faraday Trans. 2* **78** (7), 1091–1100.

SOLOMENTSEV, Y. & ANDERSON, J. L. 1994 Electrophoresis of slender particles. *J. Fluid Mech.* **279**, 197–215.

YARIV, E. 2008 Slender-body approximations for electro-phoresis and electro-rotation of polarizable particles. *J. Fluid Mech.* **613**, 85–94.

YARIV, E., SCHNITZER, O. & FRANKEL, I. 2011 Streaming-potential phenomena in the thin-Debye-layer limit. Part 1. General theory. *J. Fluid Mech.* **685**, 306–334.

https://doi.org/10.1017/jfm.2013.43 Published online by Cambridge University Press